5-1-2018

Routine Million-Particle Simulations of Epoxy Curing with Dissipative Particle Dynamics

Stephen Thomas
Boise State University

Monet Alberts
Boise State University

Michael M. Henry
Boise State University

Carla E. Estridge
Boeing Company

Eric Jankowski
Boise State University

Electronic version of an article published as:
Journal of Theoretical and Computational Chemistry, 17(3), 2018, 1840005. doi: 10.1142/S0219633618400059

Routine million-particle simulations of epoxy curing with dissipative particle dynamics

STEPHEN THOMAS
Micron School of Materials Science and Engineering, Boise State University
Boise, ID, 83725, USA

MONET ALBERTS
Micron School of Materials Science and Engineering, Boise State University
Boise, ID, 83725, USA

MICHAEL M HENRY
Micron School of Materials Science and Engineering, Boise State University
Boise, ID, 83725, USA

CARLA E ESTRIDGE
The Boeing Company
St. Louis, MO, 63134, USA

ERIC JANKOWSKI
Micron School of Materials Science and Engineering, Boise State University
Boise, ID, 83725, USA
ericjankowski@boisestate.edu

Mesoscale simulation techniques have helped to bridge the length scales and time scales needed to predict the microstructures of cured epoxies, but gaps in computational cost and experimental relevance have limited their impact. In this work we develop an open-source plugin `epoxpy` for HOOMD-Blue that enables epoxy crosslinking simulations of millions of particles to be routinely performed on a single modern graphics card. We demonstrate the first implementation of custom temperature-time curing profiles with dissipative particle dynamics and show that reaction kinetics depend sensitively on the stochastic bonding rates. We provide guidelines for modeling first-order reaction dynamics in a classic epoxy/hardener/toughener system and show structural sensitivity to the temperature-time profile during cure. We conclude with a discussion of how these efficient large-scale simulations can be used to evaluate ensembles of epoxy processing protocols to quantify the sensitivity of microstructure on processing.

Keywords: polymer, epoxy, high-throughput, DPD

1. Introduction

Epoxy thermosets are widely used in industrial applications as adhesives and coatings[1], for encapsulated electronics[1], and as matrices for advanced carbon fiber composite materials[2,3]. The widespread use of epoxies derives from the low cost precursor components and the ease with which they may be cured into materials with high chemical resistance, high strength, and low density[4]. During cure, epoxy monomers are mixed with monomers of hardening agents, reacting to form a crosslinked network that transforms from a liquid to a gel, and finally to a vitrified glass phase[5–7]. The highly crosslinked topology of the epoxy-hardener network gives the thermoset excellent hardness and thermal stability, but with low ductility and low fracture toughness[8]. In order to enhance the fracture toughness, thermo*plastic* toughening agents are added[6,8–11]. Cure-induced phase separation of toughener from reacting epoxy and amine suggests that thermoset morphology depends on how fast polymerization-induced phase separation occurs in relation to glassy vitrification[12]. To engineer composites from toughened epoxy thermosets with customizable mechanical properties, we require a fundamental understanding of how the cured morphology depends on its ingredients and how it was processed.

Understanding how to control epoxy morphology is important because the mechanical properties and reliability of parts made from epoxies depend sensitively on their microstructure[12,13]. Raghava studied the effects of poly(ether sulphone)(PES) molecular weight on phase separation in a tetrafunctional epoxy resin cured with aromatic anhydrides and concluded that the phase separation of the toughening agent from the epoxy matrix was a minimum condition for improved fracture toughness of the thermoset matrix[14]. At weight fractions of 10% PES toughener in a biphenyl epoxy resin, Mimura et al.[15] observed semi continuous phase separated networks with PES domain sizes of 50-80 nm which corresponded to a 60% increase in fracture toughness compared to the neat epoxy resin. At 20% PES weight fraction a continuous interpenetrating network with domain sizes of 1 μm was formed and the fracture toughness was observed to be 90% greater than the neat epoxy[15]. The differences in the fracture toughness of toughened thermosets have been attributed to the phase separated morphology[6,9–11]. Domains ranging from 5 nm to 12 μm have been observed and a number of studies have found that the largest increase in fracture corresponded to a co-continuous interpenetrating network morphology of thermoset and thermoplastic[12,13,15–17].

In addition to the composition of toughened epoxy blends, the processing pathway of the material has a significant impact on phase separation of toughening agents, making the ingredient-processing-performance parameter space complicated. Zhang et al. studied the effects of heating rate during cure on the morphology of PES toughened multifunctional epoxy systems and observed as the heating rate is increased the diameter of microphase separated PES domains increased from 9.67 μm to 11.41 μm[18]. Exploring this landscape through synthesis and processing of these materials is costly and labor-intensive and points to a clear need for predic-

tive capabilities to help narrow the scope of viable materials and processes to meet targeted materials performance.

In principle, computer simulations should be able to assist in the exploration of processing protocols, but in practice it is challenging to predict epoxy morphology because of the disparate time scales and length scales that matter. Using atomistic models to represent toughened epoxy thermoset structures is impractical because tens of millions of atoms are needed to represent structures on 100 nm length scales[12,13,15–17,19]. Recent atomistic simulations using ReaxFF and LAMMPS modeled crosslinking polymers networks of 4,284 atoms for which mechanical properties were calculated[20,21]. The cubic volumes in these simulations are around 4 nm long. More efficient polymer-specific schemes such as Polymatic[22] and template-based polymerization[23] have been devised to tackle the issue of high computational cost of atomistic reaction modelling. Both of these models generated crosslinked networks of hundreds of reactive units where system sizes reach a few nm, but these length-scales are far from the experimentally relevant length-scales (100's to 1000's of nm). These models also require customization for simultaneous diffusion dynamics. For epoxy microstructure simulations, we therefore require more coarse-grained models.

Two types of coarse-grained models have been used to model epoxy curing. The first type involves mapping specific chemical moieties within a monomer to coarse-grained beads such that a single monomer may be represented by more than one coarse-grained simulation elements, also known as "beads" in the context of polymer science. Yang et al.[24,25] represented a tetra-functional epoxy phenol novolac (EPN) monomer and bisphenol-A (BPA) monomer using an 8 bead and 3 bead CG model respectively. Komarov et al.[26] simulated the curing of cycloaliphatic epoxy resin (CAER) where the epoxy monomer and curing agent monomer were represented by a 7 site and 3 site CG model respectively. The coarse-grained beads in these models typically use an LJ-like non-bonded interaction. The nature of these "hardcore" models makes it suitable to study mechanical properties of cured epoxies since it allows for entanglements[27]. However, this very nature of "hardcore" models also make them difficult for modelling reaction induced phase seperation (RIP) of toughened epoxies due to energetic traps that prevent phase separation. The second type of coarse-graining involve mapping entire monomers to coarse-grained beads. These models have typically used either an LJ-like potential[28] or Dissipative Particle Dynamics (DPD)[19,29] for the non-bonded interactions. The DPD potential[30,31] models fluidic elements which can pass through each other making it suitable for modelling RIP in toughened epoxies. Liu et al. developed DPD simulations with stochastic bonding routines with 248,832 coarse-grained simulation elements, and achieved cures of around 80% in 1×10^6 steps[19]. Stochastic bonding routines have been successfully applied to polystyrene polymerization, where thermostat sensitivity to the bonding model was observed[29]. The work of Ref. 32 takes a similar stochastic reaction approach in DPD, but shows that the conversion profiles in simulations are orders of magnitude too fast with respect to experiments. Langeloth et

al. achieve nearly 80% cure with CG simulations accessing as much as 32×10^{-9} s and 10 nm length-scales[33,34]. Free radical living polymerization reaction kinetic sensitivity to bonding rates are shown in systems of 24,000 DPD spheres[35]. In Ref. 36 DPD simulations with 108,062 particles are carried out for 8×10^5 steps and in Ref. 37 the same procedure is used to achieve 92% crosslinking. In short, reactive models of epoxies are approaching 10-100 nm lengths and experimental cure fractions, but additional work is needed to simultaneously resolve reaction and diffusion dynamics for systems with more than a few hundred thousand particles.

To maximize experimental relevance, it is desirable for epoxy curing simulations to (1) represent dozens, if not thousands, of nanometers, (2) simultaneously model reaction and diffusion, (3) model experimental temperature-time curing profiles, and (4) allow high-throughput screening of thousands of experiments per week. Atomistic simulations cannot meet criterion 1. Criteria 2 and 3 can be met by improving or extending reaction models with mesoscale methods, and is the focus of the present work. Criterion 4 is desirable because isolated simulation trajectories are not adequate for studying nonequilibrium dynamics with equilibrium-based techniques such as DPD. That is, we require high-throughput simulations that enable calculations of uncertainties in simulated results and efficient evaluation of large parameter spaces to validate models and inform engineering processes.

In this work we implement an open-source plugin to HOOMD-Blue[38,39] that enables high-throughput simulation of crosslinking epoxy thermosets. HOOMD-Blue is a molecular dynamics engine written in C++ and CUDA with an easy to user python API. This allows users to leverage the easy to use nature of Python and the speed of graphic processing units. We fully describe our crosslinking algorithm and provide access to our plugin's source code. We characterize how different bonding rates influence the overall bonding kinetics and give guidelines for matching experimental rates. We model a classic toughened epoxy thermoset diglycidyl ether of bisphenol A (DGEBA[40]) epoxy with amine hardener 4-4'-diaminodiphenyl sulphone (DDS4-4'[41]), and PES toughener and demonstrate its morphology dependence on processing. In sum, we present a new computational tool that enables for the first time high throughput simulations representing millions of atoms over tens of millions of steps that achieve over 95% cure in a few hours.

2. Methods

We implement an open-source (GNU General Public License v3.0) dynamic bonding plugin that stochastically adds epoxy-amine bonds during dissipative particle dynamics performed with the HOOMD-Blue simulation engine. The source code is available at `https://bitbucket.org/cmelab/epoxpy`[42].

2.1. *HOOMD-Blue*

High-throughput molecular simulations now routinely leverage graphics processing units (GPUs) to parallelize and therefore speed up computational bottlenecks.

Packages including HOOMD-Blue, LAMMPS, and AMBER have demonstrated speedups between 2x to 10x, depending on which systems are used as benchmarks and how many core kernels are parallelized[38,43–45]. We use HOOMD-Blue to perform the DPD simulations implemented here. HOOMD-Blue is used here for its combination of performance, accessibility, and extendibility. After initializing on the CPU, HOOMD-Blue simulations with thousands to millions of simulation elements can easily be performed on a single modern GPU (e.g., NVIDIA Tesla K20 or P100) with negligible communication to the host CPU. This ability to perform large-scale simulations on a single hardware accelerator is favorable for high-throughput simulation studies on modern supercomputers. Modern supercomputers with multiple GPUs per CPU enable multiple, asynchronous molecular simulations to be performed in parallel on a single node. Because HOOMD-Blue is an importable python module the scientific computing capabilities of other python libraries (e.g. `numpy` and `scipy`) are easily leveraged for structuring simulation set-up and analysis.

While python enables quick implementation of complex modeling ideas, oftentimes performance improvements to python routines can be realized by using machine code optimized and compiled for specific hardware. HOOMD-Blue's plugin API makes it relatively straightforward to add C++ or CUDA routines that impose constraints or add functionality to molecular simulations. In this work we describe performance improvements necessary for high-throughput simulations of reacting epoxies via python and C++ implementations of our dynamic bonding algorithm.

2.2. *Dissipative particle dynamics*

We model reacting mixtures of DGEBA, DDS and PES toughener using coarse-grained representations and dissipative particle dynamics[19,30]. Difunctional DGEBA epoxides are modeled with a single coarse-grained simulation element ("bead"), as are tetrafunctional amine molecules, and monomers of PES (Figure 1). Each bead is a spherical simulation elements of the same size (diameter = 1σ). Here we consider PES chains of 10 repeat units. Throughout this work we will use the colors red, blue, and green to distinguish these three chemical species, respectively (A=amine=red, B=epoxy=blue, C=toughener=green). Throughout this work we consider equifunctional blends of amine and epoxy, with one 10-mer chain of C per 10 beads of A, so the overall species ratios A:B:C are 1:2:2, or 20% A, 40% B, and 40% C.

The DPD implementation in HOOMD-Blue[46] provides parallel force calculations and position integrations of the method originally developed by Hoogerbrugge and Koelman[30]. The force on bead i from neighbors j (where $r_{ij} \leq 1$) depends on three types of forces (Equation 1).

$$F_i = \sum_{i \neq j} F_{ij}^C + F_{ij}^R + F_{ij}^D \tag{1}$$

The conservative force

$$F_{ij}^C = a_{ij}\omega^C(r_{ij})\hat{\mathbf{r}}_{\mathbf{ij}} \tag{2}$$

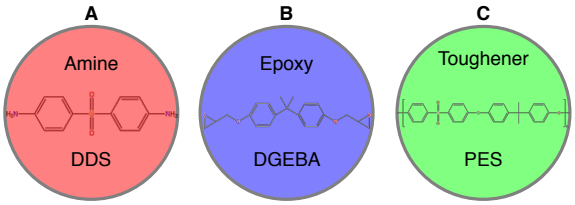

Fig. 1: Amine, epoxy, and toughener monomers are represented with spherical simulation elements ("beads").

is a soft repulsive force along the center-to-center vector $\hat{\mathbf{r}}_{\mathbf{ij}}$, where $\mathbf{r_{ij}} = \mathbf{r_i} - \mathbf{r_j}$, $r_{ij} = |\mathbf{r_{ij}}|$ and $\hat{\mathbf{r}}_{\mathbf{ij}} = \mathbf{r_{ij}}/|\mathbf{r_{ij}}|$. The force has a maximum value of a_{ij} and ω^C is a weight function, typically

$$\omega^C(r_{ij}) = \begin{cases} 1 - \frac{r}{r_{ij}} & (r \leq r_c) \\ 0 & (r > r_c) \end{cases} \tag{3}$$

,where $r_c = 1$ is the bead center-to-center cutoff distance past which beads do not interact. This linearly ramping soft repulsive force makes it easy to initialize random configurations for polymer systems and allows for relatively large timesteps ($dt \leq 0.04$)[31].

The random force

$$F_{ij}^R = \sigma\omega^R(r_{ij})\zeta_{ij}\Delta t^{-1/2}\hat{\mathbf{r}}_{\mathbf{ij}} \tag{4}$$

models random fluctuations due to thermal noise and the dissipative force

$$F_{ij}^D = -\gamma\omega^D(r_{ij})(\hat{\mathbf{r}}_{\mathbf{ij}}.\mathbf{v_{ij}}) \tag{5}$$

models viscous drag. The amplitudes σ and γ of the random and viscous forces, respectively, are related to each other by the fluctuation-dissipation theorem $\sigma^2 = 2\gamma k_B T$[47].

Here we determine the repulsion parameters a_{AA}, a_{AB}, a_{AC}, a_{BB}, a_{BC}, and a_{CC} from atomistic molecular dynamics simulations. Solubility parameters

$$\delta_i = \sqrt{E_{coh}^i/V_i} \tag{6}$$

are calculated from the cohesive energy density E_{coh} and specific volume V_i of molecules in atomistic NPT simulations equilibrated at 11 temperatures ranging from 273 K to 600 K (Appendix A). These data are used to solve for the Flory-Huggins interaction parameters

$$\chi_{ij} = \frac{\overline{V}}{k_B T}(\delta_i - \delta_j)^2 \tag{7}$$

and the DPD interaction parameters

$$a_{ij} = \frac{75 k_B T}{\rho_n} + \Delta a \tag{8}$$

via an empirical relationship

$$\chi_{ij} = 0.286\Delta a \tag{9}$$

determined for number density $\rho_n = 3$, which we also employ here[31].

The morphologies obtained with all-atom MD simulations using the OPLS-2005 force field are then compared with that of the coarse grained DPD model for validation[48]. The DPD interaction parameters averaged over the temperatures sampled between 273 K and 600 K are used here (Table I). The mass unit $M = 278.82$ g/mol is calculated from the weighted average of the masses of the A, B and C beads $\overline{M} = M_A * \phi_A + M_B * \phi_B + M_C * \phi_C$, where $M_A = 248.3$ g/mol, $M_B = 340.42$ g/mol, and $M_C = 232.46$ g/mol. Ratios of A:B:C are 1:2:2 throughout this work.

Table I: Repulsion parameters a_{ij} for amines (A), epoxies (B), and toughener (C) beads determined by Hildebrand solubility parameters from atomistic molecular dynamics.

	A	B	C
A	25.000	30.729	25.003
B		25.000	30.532
C			25.000

The average volume $\overline{V}$ is calculated as $\overline{M}/\overline{\rho}$ for the temperature of interest. The length scale is calculated as $L = (\overline{V}\rho_n)^{1/3}$ where ρ_n is the reduced number density of beads. The energy unit k_BT used here corresponds to $T_C = 439$ K. The fundamental units of energy, mass and distance are 0.873 kcal/mol, 272.82 g/mol, and 1.06 nm, respectively, where the calibration temperature $T_C = 439.36$ K. The derived units of time (τ) and force (F) are 9.29 ps and 5.7e-12 N respectively.

We use `signac` and `signac flow` for data collection and job submission[49,50]. DPD simulations are initialized using `mBuild`[51] followed by a 5000-step NVE simulation at 1760 K to generate unique random configurations for each run. Velocity distributions consistent with the starting temperature of a desired run are then set. Bonds between toughener monomers and between epoxies and amines are modeled with harmonic springs, with $k_{\text{harmonic}} = 4k_BT/r_c^2$ and equilibrium spacing $r_0 = 0$ as in Ref. 52 and Ref. 53. We employ velocity-Verlet integration of Newton's equations of motion ($dt = 0.01$) in the NVE ensemble[54]. Unless otherwise stated, the fiducial simulation parameters listed in Table II describe each simulation in this work.

2.3. *Reaction model*

Epoxy-amine crosslinking is modeled by the addition of bonds during DPD simulations, similar to the method of Liu et al. (Algorithm 1)[19]. Every τ_B steps we call the bonding routine, wherein a fraction $I = \frac{n_B}{N_B}$ of the number of the total creatable

Table II: Fiducial simulation parameters

N	50,000
L	25.54 σ
dt	0.01 τ
ρ_n	3
γ	4.5 M/τ
k_{harmonic}	4 $k_B T_C / r_c^2$
r_0	0 σ
n_B	0.000025 N_B
τ_B	1 dt
E_a	1 $k_B T_C$

bonds N_B are added (Figure 2). The bonding reactions occur stochastically as in

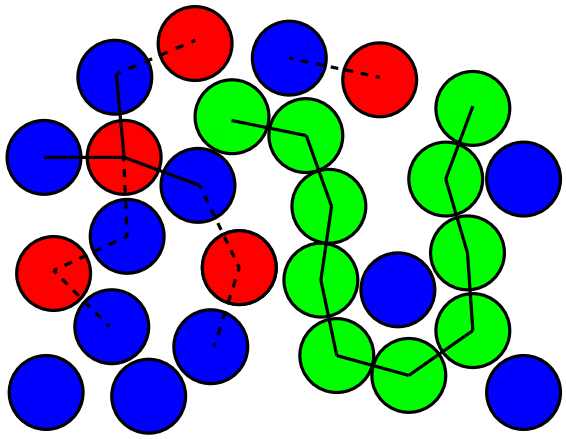

Fig. 2: During a bonding step, candidate bonds (dashed lines) are stochastically converted to bonds (solid lines) between amine/epoxy pairs that have reactive sites remaining and are sufficiently close.

Refs. 19 and 29, where the probability of forming a bond

$$p(E_a) = e^{-\frac{E_a \alpha}{k_B T}} \tag{10}$$

depends on the activation energy E_a. Here, α describes the relative activation energy of secondary (and higher order) reactions to primary bond formation

$$\alpha = \begin{cases} 1 & \text{if } [R(p_i) \; or \; R(p_j)] < 1 \\ \alpha_2 & \text{otherwise} \end{cases} \tag{11}$$

, where $R(p_X)$ gives the bond rank of particle p_X. Here, $\alpha_2 = 3$.

Algorithm 1 Amine-Epoxy bonding

1: $n_B \geq 1$, $\tau_B \geq 1$
2: **repeat** every τ_B time steps
3: **for** each bond attempt i in n_B **do**
4: p_i is a randomly chosen particle of type A or B
5: **if** p_i can bond **then**
6: Distance sort neighbors of complimentary type to p_i
7: **for** each neighbor p_j **do**
8: **if** p_j can bond and $dist(p_i, p_j) < r_{bond}$ **then**
9: Calculate $p(E_a, \alpha)$ using Equation 10 and Equation 11
10: **if** $p(E_a) > random(0, 1)$ **then**
11: Bond p_i and p_j
12: break
13: **end if**
14: **end if**
15: **end for**
16: **end if**
17: **end for**
18: **until** $t == t_{end}$

The *dist* function in line 8 gives the distance between the particles p_i and p_j. *random* in line 10 produces a uniform random number between 0 and 1.

3. Results

We perform DPD simulations of reacting epoxy thermosets with three aims. First, we identify the minimum system size necessary to observe toughener phase separation using simulated scattering experiments. Second, we vary A to determine which bonding frequencies best match experimental reaction kinetics. Third, we test two curing protocols and demonstrate morphological sensitivity to processing.

We also profiled the performance of three implementations of Algorithm 1 to optimize its performance while attempting the least amount of coding. After optimization, simulations with $N = 5 \times 10^4$ achieve 95% cure in about 45 wall-clock minutes and the $N = 2 \times 10^6$ simulations achieve 95% cure in about 7.5 wall-clock hours. We note that this ability to simulate large simulation volumes in reasonable amounts of time enabled the identification of a minimum system size necessary to observe microstructural features using this model. A detailed description of performance profiling and optimization strategies we employ are given in the Supplementary Information (SI).

3.1. *Morphology Characterization*

We characterize the degree of toughener phase separation by inspecting the C-C structure factor at low wave number, calculated using `diffractometer` from Ref. 55. Five independent replicate simulations with system sizes between 5×10^4 and 3×10^6 were run using the fiducial parameters (Table II) to obtain these C-C structure factors. Figure 3 summarizes our finding that large simulation volumes are needed to observe the length scales over which phase separation occurs by comparing C-C structure factors. In all seven cases 95% cure fraction is achieved, but the ≈ 35 nm-wide toughener domains in the $N \geq 1 \times 10^6$ simulations appear as macrophase separation occurring in the $N \leq 5 \times 10^5$ cases where the simulation volume is not large enough to resolve 35 nm features.

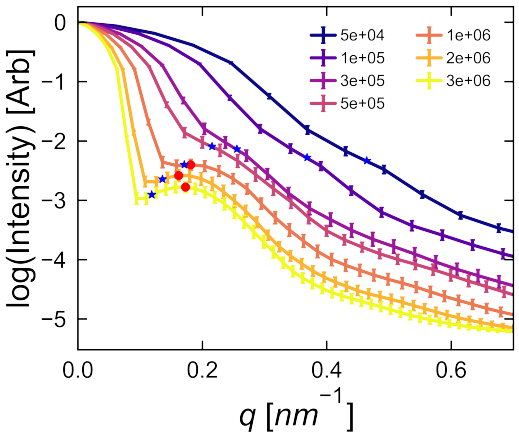

Fig. 3: C-C structure factors show ≈ 35 nm toughener domains emerge for $N > 1 \times 10^6$ system sizes, while $N = 5 \times 10^4$ systems demonstrate macrophase separation. Blue stars indicate the wavenumber corresponding to half the box length (the largest resolvable length scale with a periodic simulation volume), and red dots indicate local scattering maxima corresponding to the phase-separated feature size. The error bars indicate standard error.

Figure 4 reveals the average feature size($\langle q_{max} \rangle$) of this system to be 0.17 nm^{-1} or 37 nm. In order to resolve this feature size using the `diffractometer`, it is necessary to have a system with $L/2 \geq 37$ nm which is satisfied by $N \geq 1.2 \times 10^6$. The fact that this feature size remains intact over a large range of system sizes indicate that this is a characteristic size of this model and not a simulation artifact.

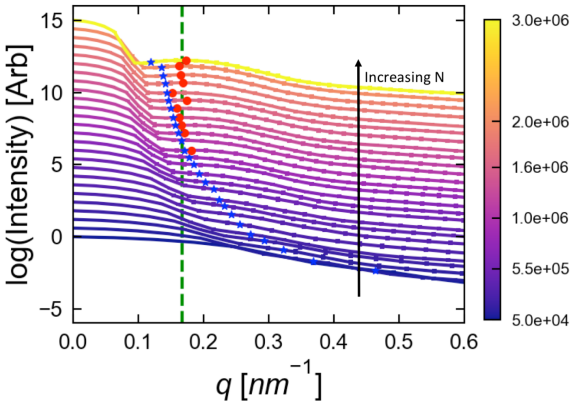

Fig. 4: C-C structure factors for $N = 5{\times}10^4$ to $N = 3{\times}10^6$ show that microstructure can consistently be detected for $N \geq 1.2 \times 10^6$. The blue stars indicate the wave vector corresponding to the half box length and the red dot indicates the detected first peak. The structure factor intensities are shifted up in intensity for visibility. The average wave vector corresponding to the characteristic feature size ($\langle q_{max} \rangle = 0.17 nm^{-1}$) is shown in dotted line and the color bar indicates N.

These results show that co-continuous domains of thermoset and thermoplastic can be efficiently simulated with the coarse-grained model and bonding algorithm used here. We pause to emphasize that these particular feature sizes and morphologies are not meant to be predictive for DGEBA/DDS/PES, because the model used here lacks key features specific to those chemistries, but serves as a qualitative validation that features important to epoxies are accessible. The 37 nm toughener domains observed here are a factor of 40 smaller than the micron-scale domains observed in some experiments, but represent the largest domains observed to date in reactive DPD models. This discrepancy in system sizes for microstructure detection reinforces the importance of large-scale volumes for predicting these morphological features.

3.2. *Calibration of Reaction Kinetics*

Simulation of bonding dynamics with coarse-grained models requires the simulated reaction kinetics to be matched to experimental time scales. The reaction rate constant

$$k = He^{\frac{-E_a}{RT}} \tag{12}$$

depends on the reaction activation energy E_a and prefactor H. Due to the accelerated dynamics in coarse-grained models, it is not necessarily the case that experimentally-determined E_a and H will model the desired kinetics in a model

trajectory. The degree of cure X measures the fraction of possible bonds that have formed in a curing epoxy, and its rate of change

$$\frac{dX}{dt} = k(t)f(X) \tag{13}$$

is modeled by the k and $f(X)$, which is a polynomial in X describing reaction kinetics[56]. For example, $f(X) = X_\infty - X$ for first-order (FO) reaction kinetics, $f(X) = (X_\infty - X)^2$ for second-order (SO), $f(X) = (X_\infty - X)(1 + CX)$ for self-accelerated first-order (SAFO), and $f(X) = (1-X)(X_\infty - X)(1+CX)$. Here, X_∞ is the degree of cure at $t = \infty$ and C is a temperature-independent acceleration constant. In the reaction model implemented here, the prefactor H is related to the number of bonds we attempt per call to the bonding routine (n_B) and the steps between bonding routine calls (τ_B).

To determine reaction sensitivity to the ratio $A = \frac{n_B}{\tau_B}$, we perform high-throughput DPD simulations with dynamic bonding. Isothermal curing simulations are performed until $\alpha_\infty = 0.95$ is achieved, using the fiducial parameters, except n_B, τ_B and k_BT are varied. The number of bonds to attempt per bonding-step is expressed as a fraction of the total number of bonds (N_B) that can be formed from initial concentrations of amines and epoxy monomers. Here, $n_B \in \{0.000025N_B, 0.00005N_B, 0.0001N_B, 0.01N_B\}$, $\tau_B \in \{1, 2, 10, 20, 40, 80, 100\}$, and $k_BT \in \{0.2, 0.5, 1, 2, 3, 4, 5, 6\}$, for a total of 224 parameter combinations. At each parameter combination we perform twenty repeat trials, for a total of 4480 calibration simulations performed over three weeks. After each simulation completes, the cure profile $X(t)$ is fit with FO, SO, SAFO, and SASO models and the mean square deviation R^2 is calculated for each of the four models. A representative cure profile and associated amine concentrations is shown in Figure 5. The Python plotting library `Matplotlib` is used to generate the plots within this work[57]. For a given bonding rate A we average the R^2 across the simulated temperatures to get an aggregate measure $\langle R^2 \rangle$ for how well each kinetic model matches simulated reaction kinetics.

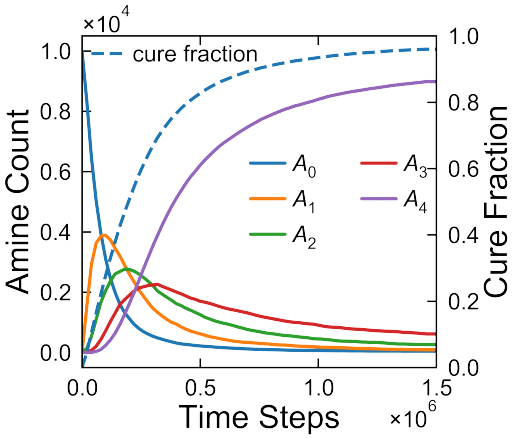

Fig. 5: Representative cure fraction (dashed) and amine concentration trajectories. A_n indicates an amine with n formed bonds.

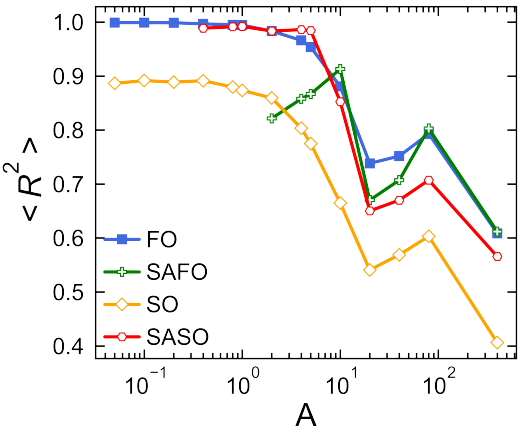

Fig. 6: Average fit metric $\langle R^2 \rangle$ for the four kinetic models as a function of bond frequency $A = \frac{n_B}{\tau_B}$.

Figure 6 summarizes kinetic model sensitivity to bonding rate A. We find the first-order kinetic model matches our simulation results near perfectly, and has the best fit when $A \leq 1$. It is expected that the FO model would best fit our reaction model because we do not model heat release with each formed bond and

because equimolar ratios of unbonded A and B are maintained as the reaction proceeds. We note that experimentally, we would expect the exothermic reactions of the amine and epoxy modeled here to give rise to SASO kinetics[56]. With the exception of the SASO model, the general trend is towards higher accuracy fits with lower A. The observation that simulated bonding kinetics so sensitively depend on A suggests that coarse-grained simulations of dynamically crosslinked epoxies require characterization and justification of stochastic bond frequencies. The sensitivity of bonding kinetics to A is highlighted between Figure 7(a) and Figure 7(b), where changing A from 2 to 0.1 causes cure fractions drop significantly over the same time scale. For the first order reaction model we find a general trend of improved accuracy with smaller A(Table III). When $A \leq 1$, the average quality of fit is greater than 0.9945, but rapidly decreases for $A > 1$. We find that the accuracy of the FO model is best for temperatures close to the calibration temperature $0.5k_BT_C < k_BT < 4k_BT_C$. We note that the optimal A values obtained in this study are sensitive to the time step (dt). Further studies will aim to explore the sensitivity of A to dt.

Again we emphasize that $A < 1$ is not necessarily the optimal choice for modeling DGEBA/DDS crosslinking, but that reaction kinetics can be calibrated to desired experimental kinetics with high throughput simulations. A fundamental challenge with using DPD to simultaneously model reaction and diffusion arises from the fact that particles diffuse as fast as momentum, rather than a factor of 1000 slower[31], so simulation timescales derived from mass, distance, and energy are not straightforward to interpret. The ability to independently tune reaction timescales with bonding frequency A and diffusion timescales with γ offer promise for developing reactive DPD simulations that are at least empirically informed and predictive, if not broadly transferable.

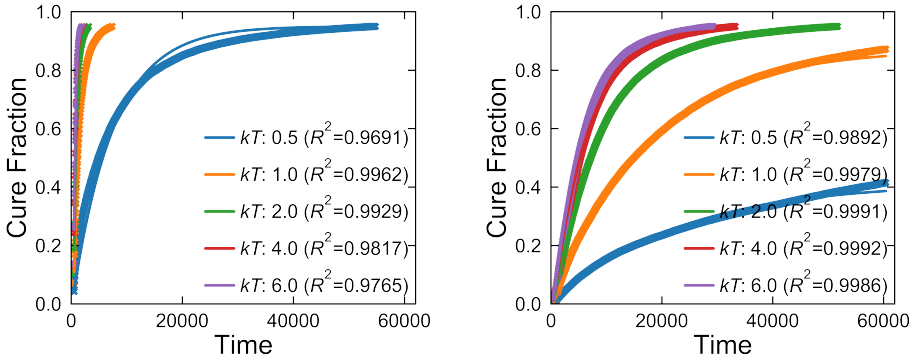

(a) $A = 2.0$ (b) $A = 0.1$

Fig. 7: FO model fits of simulated X_T for (a) $A = 2.0$ and (b) $A = 0.1$. Reducing A increases R^2 and decreases X_T.

Table III: Fit quality (R^2) for the FO model

A	k_BT	Best τ_B	Best n_B (Fraction of N_B)	H	R^2	$< R^2 >$
	0.5	40	1.0e-4	0.0164	0.9823	
	1.0	40	1.0e-4	0.0081	0.9979	
0.1	2.0	20	5.0e-4	0.0090	0.9991	0.9954
	4.0	10	2.5e-5	0.0100	0.9992	
	6.0	20	5.0e-5	0.0103	0.9986	
	0.5	5	5.0e-4	0.0194	0.9793	
	1.0	10	5.0e-4	0.0251	0.9928	
0.4	2.0	10	1.0e-4	0.035	0.9992	0.9932
	4.0	10	1.0e-4	0.0389	0.9979	
	6.0	5	1.0e-4	0.04	0.9970	
	0.5	5	1.0e-4	0.0262	0.9785	
	1.0	5	1.0e-4	0.0491	0.9932	
0.8	2.0	5	1.0e-4	0.0672	0.9983	0.9917
	4.0	5	1.0e-4	0.0745	0.9954	
	6.0	5	1.0e-4	0.0764	0.9932	
	0.5	1	2.5e-5	0.0297	0.9759	
	1.0	1	2.5e-5	0.0611	0.9947	
1.0	2.0	1	2.5e-5	0.0830	0.9978	0.9907
	4.0	1	2.5e-5	0.0910	0.9943	
	6.0	1	2.5e-5	0.0940	0.9910	
	0.5	1	5.0e-4	0.0495	0.9691	
	1.0	1	5.0e-4	0.1155	0.9962	
2.0	2.0	1	5.0e-4	0.1538	0.9929	0.9832
	4.0	1	5.0e-4	0.1662	0.9817	
	6.0	1	5.0e-4	0.1691	0.9765	
	0.5	100	1.0e-2	0.0943	0.9776	
	1.0	1	4.0e-2	0.2142	0.9959	
4.0	2.0	100	1.0e-2	0.2650	0.9774	0.9661
	4.0	100	1.0e-2	0.2743	0.9464	
	6.0	100	1.0e-2	0.2729	0.9333	
	0.5	80	4.0e-2	0.1165	0.9791	
	1.0	80	4.0e-2	0.2555	0.9943	
5.0	2.0	80	4.0e-2	0.3114	0.9646	0.9537
	4.0	80	4.0e-2	0.3140	0.9260	
	6.0	80	4.0e-2	0.3151	0.9045	
	0.5	40	4.0e-2	0.2157	0.9879	
	1.0	40	4.0e-2	0.4407	0.9785	
10.0	2.0	40	4.0e-2	0.4646	0.8940	0.8808
	4.0	40	4.0e-2	0.4429	0.7945	
	6.0	40	4.0e-2	0.4293	0.7490	

3.3. *Cure Path Dependence*

Two temperature profiles are tested to characterize how structural evolution of epoxy networks depend on the temperature history during cure (Figure 8). Isothermally cured samples are initialized at the cure temperature and maintained there throughout the simulation (1×10^7 steps). Linearly ramped samples are initialized at 300 K and then linearly heated to the final cure temperature over 1×10^7 steps. The bonding is stopped when the sample is cured 95 % ($X_{cut} = 0.95$). The linearly ramped simulation at 850 K reaches this cure fraction at $\approx 5 \times 10^6$ timesteps as seen in Figure 8. Curing simulations with each temperature profile are performed with fiducial simulations with the exception of E_a=2 $k_B T_C$ at each of five final temperatures $T \in \{200, 425, 600, 850, 1000\}$ K. Ten independent replicate simulations are performed at each cure temperature for both temperature profiles to quantify uncertainties.

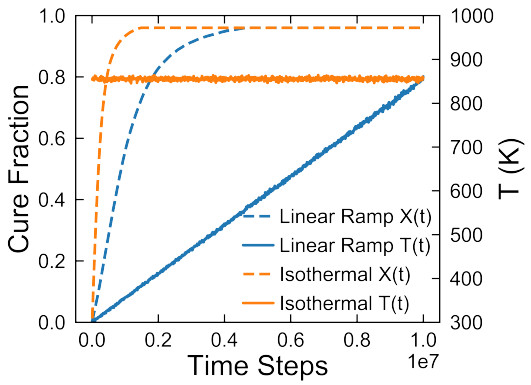

Fig. 8: Isothermal curing results in higher cure fraction as a function of time during the first half of the simulation at 850 K, while linear ramps allow for more structural rearrangements at the point each cure protocol reaches the same cure fraction.

As expected, the lower average temperature of the linearly ramped cures results in lower curing at fixed cure time before reaching X_{cut} as seen in Figure 8.

In each simulation we monitor the sizes of the largest and second largest molecules using `NetworkX`[58]. In simulations where the molecular weights of these two molecules diverge, we deem the divergence time the *gel point*. The largest and second-largest molecule sizes are useful metrics for measuring gelation because once a percolating cluster exists it is more likely for clusters to bond to the percolating cluster than to grow independently. Therefore, a divergence in the first and second largest cluster sizes is a good proxy for when a percolating cluster exists. Average final cure percentages and gel points for each temperature are shown in Figure 9.

Both profiles show $X_{gel} \approx 0.5$ for all temperatures. It is expected that X_{gel} should depend on the functionality and initial concentrations of the reacting molecules, but be independent of temperature and processing.[56,59] Gelation for the chemical species considered in our model is known to occur experimentally around 0.6 cure fraction[59,60] and this property is a consequence of the percolation threshold. The X_{gel} reported here are lower than expected for with DGEBA/DDS blends. Because our current dissipative dynamics do not capture chain entanglements and because we omit the exothermic reaction effects it is not surprising that X_{gel} does not precisely match experiments. At a low temperature of 200 K,the energetic favorability of amines to prefer mixing with tougheners rather than with epoxy(Table I), in combination with the slower diffusion of particles from a fully mixed initial condition, the linear ramp curing resulted in a higher cure fraction(Figure 9).

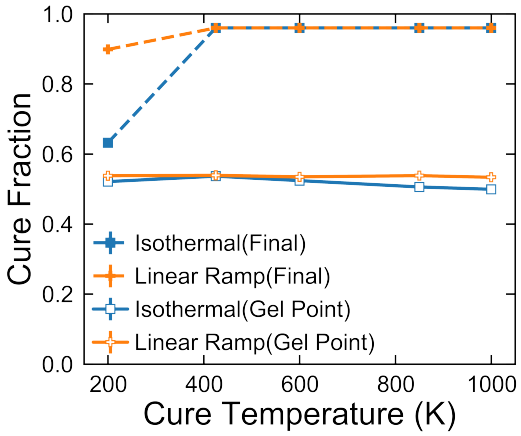

Fig. 9: Except for 200 K, all the samples reach $X_{cut} = 0.95$. We observe $X_{gel} \approx 0.5$ for all temperatures.

Figure 10(b) shows that the isothermal cures give rise to larger feature sizes than the linear ramped case where the toughener completely phase separate from the resin. As expected, the standard error of structure factors for the macro phase separated samples in Figure 10 are lesser than the samples which are not macro phase separated.

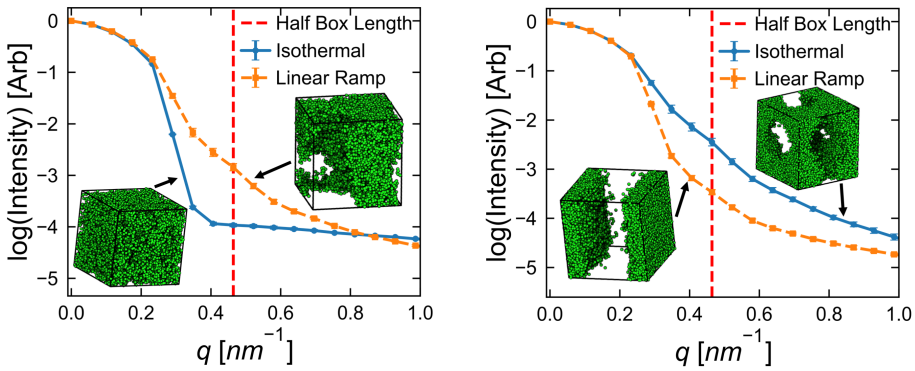

(a) Cure Fraction = 0.10 (b) Cure Fraction = 0.95

Fig. 10: Structure evolves differently for the samples cured with different temperature profiles. C-C structure factors are shown for samples taken at 10% cure and 95% cure. The error bars show standard error.

We observe differences in how structures evolve between the isothermal and linear ramp cures. At 10% cure, the linearly cured samples have larger feature sizes compared to the isothermally cured samples based on the higher intensity at low wave numbers(Figure 10(a)). This is in contrast to the final structures for the two curing protocols, where isothermal cure results in larger sized features.

The observation that two different temperature histories give rise to different morphologies at the same cure fractions is important because this is a qualitative modeling feature needed to understand via simulations how processing influences structure. The low standard error for the structure factors further reinforce that the temperature histories curing a cure cycle has a strong influence on the resultant microstructure. The ability to set generic temperature-time histories for curing epoxies at 90 nm length scales enables the application of high throughput simulations to this problem of industrial interest. Cure path sensitivities reported here are not expected to hold for DGEBA/DDS/PES systems in particular, though we expect calibrated models using the techniques reported here will advance towards being predictive.

4. Conclusions

DPD simulations of millions of reacting particles can be performed with experimentally-relevant temperature profiles in a few hours using `epoxpy` and HOOMD-Blue on K20 and P100 GPUs from NVIDIA. Even though the bonding algorithm is written specifically as a plugin for HOOMD-Blue, it should be fairly straightforward to implement it in other MD tools such as LAMMPS as long they permit adding bonds on-the-fly and provides access to their neighborlist. Given the

object-oriented nature of `epoxpy`, extending it for other MD packages is also feasible. With coarse-grained beads representing reactive monomers, million-particle simulations approach representation of cubic volumes with 100 nm sides, and desired reaction kinetics can be tuned by adjustment of the stochastic bonding rates, an essential validation step. Here we find that to match first order reaction kinetics, very small bond rates (0.002% of possible bonds) are required. Irrespective of the kinetic model, our findings support the heuristic that low bonding rates are necessary to match cure kinetics because of the fast transport enabled by DPD. These observations inform a possible two-step process for calibrating nonequilibrium bonding simulations of reactive polymers: (1) Match cure kinetics to experiments with stochastic reaction rates, and (2) use the dissipative drag parameter γ to match structural relaxation times. We demonstrate the present model captures temperature history dependence on microstructure, that co-continuous domains spontaneously phase separate of crosslinking with gelation transitions that all qualitatively match experiments. We also find that a minimum system size of 1.2×10^6 particles is necessary to clearly detect the peak in the C-C structure factor which characterizes microphase separation. With this ability to capture the relevant structure and dynamics of crosslinking polymers, future work will focus on developing and validating models for specific reacting systems and incorporating interaction potentials that enable chain entanglements to be modeled.

5. Acknowledgements

This material is based upon work supported by The Boeing Company under contract BRT-LO217-0072. This material is based upon work supported by the National Science Foundation under Grant No. 1229709. MMH was supported by a NASA Idaho Space Grant Consortium fellowship, which is funded by NASA (NNX15Ai04H).

References

1. *Epoxy Resin Market Analysis By Application (Paints & Coatings, Wind Turbine, Composites, Construction, Electrical & Electronics, Adhesives) And Segment Forecasts To 2024*, *Tech Rep* 978-1-68038-171-9, Grand View Research, URL http://www.grandviewresearch.com/industry-analysis/epoxy-resins-market.
2. Soutis C, Carbon fiber reinforced plastics in aircraft construction, *Materials Science and Engineering A* **412**(1-2):171–176, 2005. doi:10.1016/j.msea.2005.08.064.
3. Timmis AJ, Hodzic A, Koh L, Bonner M, Soutis C, Schäfer AW, Dray L, Environmental impact assessment of aviation emission reduction through the implementation of composite materials, *International Journal of Life Cycle Assessment* **20**(2):233–243, 2015. doi:10.1007/s11367-014-0824-0.
4. Xu Y, Hoa SV, Mechanical properties of carbon fiber reinforced epoxy/clay

nanocomposites, *Composites Science and Technology* **68**(3-4):854–861, 2008. doi:10.1016/j.compscitech.2007.08.013.

5. Wang X, Gillham JK, Competitive primary amine/epoxy and secondary amine/epoxy reactions. Effect on the isothermal time-to-vitrify, *Journal of Applied Polymer Science* **43**(12):2267–2277, 1991. doi:10.1002/app.1991.070431216.
6. Mimura K, Ito H, Fujioka H, Toughening of epoxy resin modified with in situ polymerized thermoplastic polymers, *Polymer* **42**(22):9223–9233, 2001. doi:10.1016/S0032-3861(01)00460-8.
7. Ming Z, Xuefeng A, Bangming T, Xiaosu Y, TTT Diagram Used to Control Phase Structure of 2/4 Functional Epoxy Blends for Advanced Composites, *Chinese Journal of Aeronautics* **22**(4):449–452, 2009. doi:10.1016/S1000-9361(08)60124-7, URL http://dx.doi.org/10.1016/S1000-9361(08)60124-7.
8. Levita G, Petris S, Marchetti a, Lazzeri a, Crosslink density and fracture toughness of epoxy resins, *Journal of Materials Science* **26**(9):2348–2352, 1991. doi:10.1007/BF01130180.
9. Iijima T, Miura S, Fukuda W, Tomoi M, Effect of cross-link density on modification of epoxy resins by N-phenylmaleimide-styrene copolymers, *European Polymer Journal* **29**(8):1103–1113, 1993. doi:10.1016/0014-3057(93)90317-9.
10. Di Pasquale G, Motto O, Rocca A, Carter J, McGrail P, Acierno D, New high-performance thermoplastic toughened epoxy thermosets, *Polymer* **38**(17):4345–4348, 1997. doi:10.1016/S0032-3861(96)01031-2, URL http://www.sciencedirect.com/science/article/pii/S0032386196010312.
11. Blanco I, Cicala G, Faro CL, Recca A, Development of a toughened DGEBS/DDS system toward improved thermal and mechanical properties by the addition of a tetrafunctional epoxy resin and a novel thermoplastic, *Journal of Applied Polymer Science* **89**(1):268–273, 2003. doi:10.1002/app.12179.
12. Yamanaka K, Inoue T, Structure development in epoxy resin modified with poly(ether sulphone), *Polymer* **30**(4):662–667, 1989. doi:10.1016/0032-3861(89)90151-1.
13. Brooker RD, Kinloch AJ, Taylor AC, The Morphology and Fracture Properties of Thermoplastic-Toughened Epoxy Polymers, *The Journal of Adhesion* **86**(7):726–741, 2010. doi:10.1080/00218464.2010.482415, URL http://www.tandfonline.com/doi/abs/10.1080/00218464.2010.482415.
14. Raghava R, Development and characterization of thermosetting-thermoplastic polymer blends for applications in damage-tolerant composites, *Journal of Polymer Science Part B: Polymer Physics* **26**(1):65–81, 1988.
15. Mimura K, Ito H, Fujioka H, Improvement of thermal and mechanical properties by control of morphologies in PES-modified epoxy resins, *Polymer* **41**(12):4451–4459, 2000. doi:10.1016/S0032-3861(99)00700-4.
16. Kim YS, Kim SC, Properties of polyetherimide/dicyanate semi-interpenetrating polymer network having the morphology spectrum, *Macromolecules* **32**(7):2334–2341, 1999. doi:10.1021/ma981083v.

17. Yu Y, Zhang Z, Gan W, Wang M, Li S, Effect of polyethersulfone on the mechanical and rheological properties of polyetherimide-modified epoxy systems, *Industrial and Engineering Chemistry Research* **42**(14):3250–3256, 2003. doi:10.1021/ie0210309, URL http://www.scopus.com/inward/record.url?eid=2-s2.0-0037999910{&}partnerID=40{&}md5=ca1fbe669aabe01f1dcd08d6b57c3e4e.
18. Zhang J, Guo Q, Fox BL, Study on thermoplastic-modified multifunctional epoxies: Influence of heating rate on cure behaviour and phase separation, *Composites Science and Technology* **69**(7-8):1172–1179, 2009. doi:10.1016/j.compscitech.2009.02.016, URL http://dx.doi.org/10.1016/j.compscitech.2009.02.016.
19. Liu H, Li M, Lu ZY, Zhang ZG, Sun CC, Cui T, Multiscale Simulation Study on the Curing Reaction and the Network Structure in a Typical Epoxy System, *Macromolecules* **44**(21):8650–8660, 2011. doi:10.1021/ma201390k, URL http://pubs.acs.org/doi/abs/10.1021/ma201390k.
20. van Duin ACT, Dasgupta S, Lorant F, A GW, ReaxFF: A Reactive Force Field for Hydrocarbonds, *Journal of Physical Chemistry A* **105**(41):9396–9409, 2001. doi:10.1021/jp004368u.
21. Odegard GM, Jensen BD, Gowtham S, Wu J, He J, Zhang Z, Predicting mechanical response of crosslinked epoxy using ReaxFF, *Chemical Physics Letters* **591**:175–178, 2014. doi:10.1016/j.cplett.2013.11.036, URL http://dx.doi.org/10.1016/j.cplett.2013.11.036.
22. Abbott LJ, Hughes JE, Colina CM, Virtual synthesis of thermally cross-linked copolymers from a novel implementation of polymatic, *Journal of Physical Chemistry B* **118**(7):1916–1924, 2014. doi:10.1021/jp409664d.
23. Gissinger JR, Jensen BD, Wise KE, Modeling chemical reactions in classical molecular dynamics simulations, *Polymer* **128**:211–217, 2017. doi:10.1016/j.polymer.2017.09.038, URL https://doi.org/10.1016/j.polymer.2017.09.038.
24. Yang S, Qu J, Coarse-grained molecular dynamics simulations of the tensile behavior of a thermosetting polymer, *Physical Review E* **90**(1):012601, 2014. doi:10.1103/PhysRevE.90.012601, URL https://link.aps.org/doi/10.1103/PhysRevE.90.012601.
25. Yang S, Cui Z, Qu J, A coarse-grained model for epoxy molding compound, *Journal of Physical Chemistry B* **118**(6):1660–1669, 2014. doi:10.1021/jp409297t.
26. Komarov PV, Yu-Tsung C, Shih-Ming C, Khalatur PG, Reineker P, Highly Cross-Linked Epoxy Resins: An Atomistic Molecular Dynamics Simulation Combined with a Mapping/Reverse Mapping Procedure, *Macromolecules* **40**(22):8104–8113, 2007. doi:10.1021/ma070702+, URL http://dx.doi.org/10.1021/ma070702+.
27. Español P, Warren PB, Perspective : Dissipative particle dynamics, *The Journal of chemical physics* **150901**, 2017. doi:10.1063/1.4979514.

28. Mukherji D, Abrams CF, Mechanical behavior of highly cross-linked polymer networks and its links to microscopic structure, *Physical Review E - Statistical, Nonlinear, and Soft Matter Physics* **79**(6):1–10, 2009. doi:10.1103/PhysRevE.79.061802.
29. Liu H, Zhu YL, Lu ZY, Müller-Plathe F, A kinetic chain growth algorithm in coarse-grained simulations, *Journal of Computational Chemistry* pp. 2634–2646, 2016. doi:10.1002/jcc.24495.
30. Hoogerbrugge PJ, Koelman JMVA, Simulating Microscopic Hydrodynamic Phenomena
with Dissipative Particle Dynamics, *Europhys Lett* **19**(1):155–160, 1992. doi:10.1209/0295-5075/19/3/001, URL http://stacks.iop.org/0295-5075/19/i=3/a=001?key=crossref.197c567e055a029b59860f932faf76d1http://iopscience.iop.org/0295-5075/19/3/001.
31. Groot RD, Warren PB, Dissipative Particle Dynamics: Bridging the Gap between Atomistic and Mesoscopic Simulation, *The Journal of Chemical Physics* **107**(11):4423, 1997. doi:10.1063/1.474784, URL http://aip.scitation.org/doi/10.1063/1.474784http://scitation.aip.org/content/aip/journal/jcp/107/11/10.1063/1.474784.
32. Li M, Gu YZ, Liu H, Li YX, Wang SK, Wu Q, Zhang ZG, Investigation the interphase formation process of carbon fiber/epoxy composites using a multi-scale simulation method, *Composites Science and Technology* **86**:117–121, 2013. doi:10.1016/j.compscitech.2013.07.008, URL http://dx.doi.org/10.1016/j.compscitech.2013.07.008.
33. Langeloth M, Sugii T, Böhm MC, Müller-Plathe F, Formation of the interphase of a cured epoxy resin near a metal surface: Coarse-grained reactive molecular dynamics simulations, *Soft Materials* **12**(ja):71–79, 2014. doi:10.1080/1539445X.2014.963873, URL http://dx.doi.org/10.1080/1539445X.2014.963873.
34. Langeloth M, Sugii T, Böhm MC, Müller-Plathe F, The glass transition in cured epoxy thermosets: A comparative molecular dynamics study in coarse-grained and atomistic resolution, *The Journal of Chemical Physics* **143**(24):243158, 2015. doi:10.1063/1.4937627, URL http://scitation.aip.org/content/aip/journal/jcp/143/24/10.1063/1.4937627.
35. Yong X, Kuksenok O, Balazs AC, Modeling free radical polymerization using dissipative particle dynamics, *Polymer* **72**:217–225, 2015. doi:10.1016/j.polymer.2015.01.052, URL http://dx.doi.org/10.1016/j.polymer.2015.01.052.
36. Kacar G, Peters EAJF, de With G, Mesoscopic simulations for the molecular and network structure of a thermoset polymer, *Soft Matter* **9**(24):5785, 2013. doi:10.1039/c3sm50304f, URL http://xlink.rsc.org/?DOI=c3sm50304f.
37. Kacar G, Peters EAJF, De With G, Multi-scale simulations for predicting material properties of a cross-linked polymer, *Computational Materials Science* **102**:68–77, 2015. doi:10.1016/j.commatsci.2015.02.021, URL http://dx.doi.

org/10.1016/j.commatsci.2015.02.021.

38. Anderson JA, Lorenz CD, Travesset A, General Purpose Molecular Dynamics Simulations Fully Implemented on Graphics Processing Units, *Journal of Computational Physics* **227**(10):5342–5359, 2008. doi:10.1016/j.jcp.2008.01.047, URL http://www.sciencedirect.com/science/article/pii/S0021999108000818http://linkinghub.elsevier.com/retrieve/pii/S0021999108000818.
39. Glaser J, Nguyen TD, Anderson JA, Lui P, Spiga F, Millan JA, Morse DC, Glotzer SC, Strong Scaling of General-purpose Molecular Dynamics Simulations on GPUs, *Computer Physics Communications* **192**:97–107, 2014. doi:10.1016/j.cpc.2015.02.028, URL http://arxiv.org/abs/1412.3387.
40. *National Center for Biotechnology Information. PubChem Compound Database; CID=2286*, https://pubchem.ncbi.nlm.nih.gov/compound/2286 (accessed Jul. 01, 2017).
41. *National Center for Biotechnology Information. PubChem Compound Database; CID=2955*, https://pubchem.ncbi.nlm.nih.gov/compound/2955 (accessed Jul. 01, 2017).
42. Thomas S, Henry M, Alberts M, *amburan/epoxpy: Introducing epoxpy*, 2017.
43. Anderson JA, Glotzer SC, The development and expansion of HOOMD-blue through six years of GPU proliferation, *arXiv* **1308.5587**, 2013, URL http://arxiv.org/abs/1308.5587.
44. Trott CR, *LammpsCuda-a new GPU accelerated Molecular Dynamics Simulations Package and its Application to Ion-Conducting Glasses*. PhD Thesis, 2011.
45. Götz AW, Williamson MJ, Xu D, Poole D, Le Grand S, Walker RC, Routine Microsecond Molecular Dynamics Simulations with AMBER on GPUs. 1. Generalized Born, *Journal of Chemical Theory and Computation* **8**(5):1542–1555, 2012. doi:10.1021/ct200909j, URL http://pubs.acs.org/doi/abs/10.1021/ct200909j.
46. Phillips CL, Anderson Ja, Glotzer SC, Pseudo-random number generation for Brownian Dynamics and Dissipative Particle Dynamics simulations on GPU devices, *Journal of Computational Physics* **230**(19):7191–7201, 2011. doi:10.1016/j.jcp.2011.05.021, URL http://linkinghub.elsevier.com/retrieve/pii/S0021999111003329.
47. Espanol P Warren P, Statistical Mechanics of Dissipative Particle Dynamics, *Europhysics Letters (EPL)* **30**:191, 1995, URL http://iopscience.iop.org/0295-5075/30/4/001.
48. Lubna N, Kamath G, Potoff JJ, Rai N, Siepmann JI, Transferable Potentials for Phase Equilibria. 8. United-atom Description for Thiols, Sulfides, Disulfides, and Thiophene, *The Journal of Physical Chemistry B* **109**(50):24100–24107, 2005. doi:10.1021/jp0549125, URL http://www.ncbi.nlm.nih.gov/pubmed/16375402.
49. Adorf CS, Dodd PM, Ramasubramani V, Swerdlow B, *csadorf/signac: v0.7.0*,

2017.

50. Adorf CS, Dodd PM, Glotzer SC, *signac - A Simple Data Management Framework*, 2016.
51. Klein C, Sallai J, Jones TJ, Iacovella CR, McCabe C, Cummings PT, A Hierarchical, Component Based Approach to Screening Properties of Soft Matter, *Foundations of Molecular Modeling and Simulation* , 2016. doi:http://dx.doi.org/10.1007/978-981-10-1128-3_5.
52. Ibergay C, Malfreyt P, Tildesley DJ, Interaction between two polyelectrolyte brushes: a mesoscale modelling of the compression, *Soft Matter* **7**:4900–4907, 2011. doi:10.1039/C1SM05068K, URL http://dx.doi.org/10.1039/C1SM05068K.
53. Ibergay C, Malfreyt P, Tildesley DJ, Electrostatic interactions in dissipative particle dynamics: Toward a mesoscale modeling of the polyelectrolyte brushes, *Journal of Chemical Theory and Computation* **5**(12):3245–3259, 2009. doi:10.1021/ct900296s, URL http://dx.doi.org/10.1021/ct900296s, pMID: 26602508.
54. Swope WC, Andersen HC, Berens PH, Wilson KR, A Computer Simulation Method for the Calculation of Equilibrium Constants for the Formation of Physical Clusters of Molecules: Application to Small Water Clusters, *Journal of Chemical Physics* **76**(1):637–649, 1982. doi:10.1063/1.442716, URL http://link.aip.org/link/?JCPSA6/76/637/1.
55. Jones ML, Jankowski E, Computationally connecting organic photovoltaic performance to atomistic arrangements and bulk morphology, *Mol Simul* **43**(10-11):756–773, 2017. doi:10.1080/08927022.2017.1296958, URL https://www.tandfonline.com/doi/full/10.1080/08927022.2017.1296958http://dx.doi.org/10.1080/08927022.2017.1296958.
56. Aldridge M, Wineman A, Waas A, Kieffer J, In situ analysis of the relationship between cure kinetics and the mechanical modulus of an epoxy resin, *Macromolecules* **47**(23):8368–8376, 2014. doi:10.1021/ma501441c.
57. Hunter JD, Matplotlib: A 2D graphics environment, *Computing In Science & Engineering* **9**(3):90–95, 2007. doi:10.1109/MCSE.2007.55.
58. Hagberg AA, Schult DA, Swart PJ, Exploring network structure, dynamics, and function using NetworkX, *Proceedings of the 7th Python in Science Conference (SciPy2008)*, Pasadena, CA USA, pp. 11–15, 2008.
59. Bonnet A, Pascault JP, Sautereau H, Taha M, Camberlin Y, Epoxy-diamine thermoset/thermoplastic blends. 1. Rates of reactions before and after phase separation, *Macromolecules* **32**(25):8517–8523, 1999. doi:10.1021/ma981754p.
60. Pramanik M, Fowler EW, Rawlins JW, Another look at epoxy thermosets correlating structure with mechanical properties, *Polymer Engineering and Science* **54**(9):1990–2004, 2014. doi:10.1002/pen.23749.